NASA/TM—2019-220148

A Three-Dimensional Thermodynamically Based Function for the Progressive Failure of Unidirectional Composites

H. Sam Huang
Stony Brook University, Stony Brook, New York

Evan J. Pineda
Glenn Research Center, Cleveland, Ohio

Shaoyu Hou
Stony Brook University, Stony Brook, New York

April 2019

NASA STI Program . . . in Profile

Since its founding, NASA has been dedicated to the advancement of aeronautics and space science. The NASA Scientific and Technical Information (STI) Program plays a key part in helping NASA maintain this important role.

The NASA STI Program operates under the auspices of the Agency Chief Information Officer. It collects, organizes, provides for archiving, and disseminates NASA's STI. The NASA STI Program provides access to the NASA Technical Report Server—Registered (NTRS Reg) and NASA Technical Report Server—Public (NTRS) thus providing one of the largest collections of aeronautical and space science STI in the world. Results are published in both non-NASA channels and by NASA in the NASA STI Report Series, which includes the following report types:

- TECHNICAL PUBLICATION. Reports of completed research or a major significant phase of research that present the results of NASA programs and include extensive data or theoretical analysis. Includes compilations of significant scientific and technical data and information deemed to be of continuing reference value. NASA counter-part of peer-reviewed formal professional papers, but has less stringent limitations on manuscript length and extent of graphic presentations.

- TECHNICAL MEMORANDUM. Scientific and technical findings that are preliminary or of specialized interest, e.g., "quick-release" reports, working papers, and bibliographies that contain minimal annotation. Does not contain extensive analysis.

- CONTRACTOR REPORT. Scientific and technical findings by NASA-sponsored contractors and grantees.

- CONFERENCE PUBLICATION. Collected papers from scientific and technical conferences, symposia, seminars, or other meetings sponsored or co-sponsored by NASA.

- SPECIAL PUBLICATION. Scientific, technical, or historical information from NASA programs, projects, and missions, often concerned with subjects having substantial public interest.

- TECHNICAL TRANSLATION. English-language translations of foreign scientific and technical material pertinent to NASA's mission.

For more information about the NASA STI program, see the following:

- Access the NASA STI program home page at http://www.sti.nasa.gov

- E-mail your question to help@sti.nasa.gov

- Fax your question to the NASA STI Information Desk at 757-864-6500

- Telephone the NASA STI Information Desk at 757-864-9658

- Write to:
  NASA STI Program
  Mail Stop 148
  NASA Langley Research Center
  Hampton, VA 23681-2199

NASA/TM—2019-220148

A Three-Dimensional Thermodynamically Based Function for the Progressive Failure of Unidirectional Composites

H. Sam Huang
Stony Brook University, Stony Brook, New York

Evan J. Pineda
Glenn Research Center, Cleveland, Ohio

Shaoyu Hou
Stony Brook University, Stony Brook, New York

National Aeronautics and
Space Administration

Glenn Research Center
Cleveland, Ohio 44135

April 2019

Level of Review: This material has been technically reviewed by technical management.

Available from

NASA STI Program
Mail Stop 148
NASA Langley Research Center
Hampton, VA 23681-2199

National Technical Information Service
5285 Port Royal Road
Springfield, VA 22161
703-605-6000

This report is available in electronic form at http://www.sti.nasa.gov/ and http://ntrs.nasa.gov/

A Three-Dimensional Thermodynamically Based Function for the Progressive Failure of Unidirectional Composites

H. Sam Huang
Stony Brook University
Stony Brook, New York 11794

Evan J. Pineda
National Aeronautics and Space Administration
Glenn Research Center
Cleveland, Ohio 44135

Shaoyu Hou
Stony Brook University
Stony Brook, New York 11794

Abstract

A thermodynamically-based work potential theory for modeling progressive damage for laminated, unidirectional composites assuming plane stress (2D Schapery's theory) is extended to three dimensioanl (3D). An internal state variable, S, is defined to account for the dissipated energy due to damage evolution in the form of microstructural changes in the matrix. With the stationary of the total work potential with respect to the internal state variable, a thermodynamically-consistent set of evolution equations is derived. The internal state variable is related to the transverse and shear moduli through microdamage functions. In the first part of this work, coupon specimens are prepared to conduct experiments to characterize the relations between the internal state variable and the transverse modulus as well as shear modulus. The information is subsequent used for the prediction of three point bending test. In the second part of this work, objectivity is studied. Three separate methods utilizing different definitions of a reduced internal state variable or of the order of the polynomials are used to represent the matrix microdamage functions are employed. The three methods are implemented in a user defined subroutine within a commercial finite element method software package. Results from numerical simulations of a center-notched composites panel are compared. The agreement in the maximum stress predictions among the three methods indicates that objectivity, with respect to the functional form of the microdamage functions, is satisfied.

Introduction

Development of reliable computational methods for the prediction of laminated progressive failure has advanced for decades and is an ongoing active research effort. Damage simulations in composites can be broadly divided into four categories. The first category is based on the first-ply failure criteria approach [1] which was initially developed for lamina in unidirectional composites. The disadvantage in using the first-ply failure criteria approach is that, once a failure criterion is met, the whole lamia is regarded as have failed. Neither the position, or evolution, of damage or crack can be predicted, which often leads to error in the structural failure predictions. The second approach is based on fracture mechanics where the energy release rate, defined as energy dissipated during fracture per unit of created fracture surface area, is compared against a critical energy release rate to determine whether cracks advance [2]. The third approach uses plasticity which is more appropriate for composites exhibiting ductile behavior [3], although substantial permanent deformation may not exist upon unloading of the composite. The fourth approach is progressive failure modeling based on the continuum damage mechanics (CDM) approach [4] [5] [6] [7] [8]. The advantage of the CDM approach is that it can use stress and or strain failure criteria for predicting damage initiation coupled with progressive failure evolution.

Over the past two decades, polymer textile fiber composites (TFCs) have become attractive for lightweight applications because of their inherent toughness and inexpensive manufacturing costs. Detailed introduction to TFCs can be seen in [9] and [10]. Laminated textile composites have been used in adaptive wind turbine blades [11] and in the automobile [12].

Textile fiber composites are flexible in that, the microstructure can be tailored to attain the desired, macroscopic mechanical properties.

In order to reliably and accurately predict progressive failure of textile composites, it is necessary to develop a model in which the morphology of the fiber tows is captured by explicitly modeling the weave architecture. However, from the hierarchical structure of textile composites, shown in Figure 1, it can be seen that the fiber tows locally can be treated as transversely isotropic materials. One strategy for modeling TFCs is to employ the same methods used for unidirectional composites for the fiber tows of a mesoscale model [13] [14]. Moreover, the plane stress assumption often used for unidirectional laminates does not hold locally for the fiber tows because of the tow undulations and weave architecture. Thus, a 3D, constitutive model must be developed.

Schapery proposed a thermodynamically based work potential theory for progressive failure of unidirectional composites [15]. The cited formulation utilizes a plane stress assumption for laminated plates. In Schapery's theory, the response in the fiber direction is linear, whereas damage due to microscopic cracking in the matrix affects the transverse modulus and shear modulus. Thus, the instantaneous transverse and shear moduli are functions of damage, represented with an internal state variable, accumulated during the loading. Schaperys theory has previously been implemented within the finite element method to model the tensile and compressive response of 2D, notched composite plates [7] [8].

In this paper, the plane stress formulation of Schapery's theory [15] for laminates is extended to accommodate a fully 3D stress state while maintaining the transversely isotropic assumption commonly used for unidirectional composites. The 3D theory is implemented

within the Abaqus finite element method software package via a user defined subroutine (UMAT). This numerical implementation is used to model unidirectional laminates with the intent of using it in the future for modeling progressive failure of the fiber tows in TFCs. A crux of Schaperys theory is the use of microdamage functions, obtained from coupon experiments, to relate the degraded stiffnesses to the internal state variable. There exists a great amount of flexibility in how the experimental data is fit to obtain the microdamage functions. Sicking [16] observed that the internal state variable S, which represents the matrix microdamage evolves as the cube of the applied strain. Thus, Sicking introduced a reduced internal state variable S_r, defined as $S^{\frac{1}{3}}$. Subsequently, the Young's modulus and shear modulus were defined as polynomial functions in S_r. An additional focus of the present work is to analyze and compare progressive failure predictions obtained using various forms of the matrix microdamage functions. Three different forms for the matrix microdamage functions, where the exponent that defines the reduced internal state variable and the order of the polynomial fit of the stiffness versus reduced internal state variable data are varied, are used as input in Schapery's theory. A notched composites panel is created to conduct compression simulations using the three methods. Finally, the results are compared and summary are presented.

3D formulation of Schapery's theory for unidirectional composites

Schapery proposed a thermodynamically-based work potential theory for laminated composites[15]. Over the years, the theory has been used and extended by different researchers [8],[7], [6]

to model progressive failure of laminated composites within the finite element method. An internal state variable, S, is used to describe the energy dissipated in Figure 2 due to damage or microstructural changes under loading. From experiment, it has been shown that there is negligible stiffness degradation in the longitudinal (or fiber) direction but stiffness degradation, due to damage accumulation, does occur in the transverse direction. Thus, the transverse and shear stiffnesses are not constant but are functions of the internal state of the material.

The total work potential, W_T , is the sum of the recoverable, elastic strain energy density, W_{Strain}, and the dissipated energy potential, S.

$$W_T = W_{Strain} + S \tag{1}$$

Due to the principle of stationarity of the total work potential with respect to the internal state variable, at any instant of thermodynamic equilibrium, the following equation holds

$$\frac{\partial W_T}{\partial S} = 0 \tag{2}$$

Also, the dissipated energy ,S, is not reversible. That is,

$$\dot{S} \geq 0 \tag{3}$$

Substituting Eq (1) into Eq (2), the evolution equation for laminated composites can be derived.

Assuming the local coordinate 1 is defined to align with the fiber direction, direction 2 and direction 3 are aligned with the transverse direction normal to the fiber direction. The fully

3D strain state can be expressed in terms of stress by the compliance matrix, $[C]$. That is , $\{\varepsilon\}$= $[C]$ $\{\sigma\}$ where $[C]$ is expressed as follows

$$[C] = \begin{bmatrix} \frac{1}{E_1} & \frac{-\nu_{21}}{E_2} & \frac{-\nu_{21}}{E_2} & 0 & 0 & 0 \\ \frac{-\nu_{12}}{E_1} & \frac{1}{E_2} & \frac{-\nu_{23}}{E_2} & 0 & 0 & 0 \\ \frac{-\nu_{12}}{E_1} & \frac{-\nu_{23}}{E_2} & \frac{1}{E_2} & 0 & 0 & 0 \\ 0 & 0 & 0 & \frac{(1+\nu_{23})}{E_2} & 0 & 0 \\ 0 & 0 & 0 & 0 & \frac{1}{2G_{12}} & 0 \\ 0 & 0 & 0 & 0 & 0 & \frac{1}{2G_{12}} \end{bmatrix} \tag{4}$$

The five parameters, $E_1, E_2, G_{12}, \nu_{21}, \nu_{23}$ are used to describe a transversely isotropic lamina, or fiber tow. Due to symmetry, the term $\frac{-\nu_{21}}{E_2}$ is equivalent to the term $\frac{-\nu_{12}}{E_1}$. Thus, ν_{12} is not an independent variable. By taking the inverse of the compliance matrix [C], the stiffness matrix [K] can be expressed as the following

$$\begin{bmatrix} K_{11} & K_{12} & K_{12} & 0 & 0 & 0 \\ K_{12} & K_{22} & K_{23} & 0 & 0 & 0 \\ K_{12} & K_{23} & K_{22} & 0 & 0 & 0 \\ 0 & 0 & 0 & K_{44} & 0 & 0 \\ 0 & 0 & 0 & 0 & K_{55} & 0 \\ 0 & 0 & 0 & 0 & 0 & K_{55} \end{bmatrix} \tag{5}$$

where

$$K_{11} = \frac{E_1 E_2(-1+\nu_{23})}{2E_1\nu_{21}^2 + E_2(-1+\nu_{23})} \tag{6}$$

$$K_{12} = \frac{-E_1 E_2 \nu_{21}}{2E_1\nu_{21}^2 + E_2(-1+\nu_{23})} \tag{7}$$

$$K_{22} = \frac{-E_2(E_2 - E_1\nu_{21}^2)}{(2E_1\nu_{21}^2 + E_2(-1+\nu_{23}))(1+\nu_{23})} \tag{8}$$

$$K_{23} = \frac{-E_2(E_2\nu_{23} + E_1\nu_{21}^2)}{(2E_1\nu_{21}^2 + E_2(-1+\nu_{23}))(1+\nu_{23})} \tag{9}$$

$$K_{44} = \frac{E_2}{(1+\nu_{23})} \tag{10}$$

$$K_{55} = 2G_{12} \tag{11}$$

Typically, the product of two Poisson ratios is relatively small; i.e., $\nu_{21}\nu_{21} << 1$. Thus, [K] matrix can be simplified as the following

$$[K] = \begin{bmatrix} E_1 & \frac{E_1\nu_{21}}{1-\nu_{23}} & \frac{E_1\nu_{21}}{1-\nu_{23}} & 0 & 0 & 0 \\ \frac{E_1\nu_{21}}{1-\nu_{23}} & E_2 & E_2\nu_{23} & 0 & 0 & 0 \\ \frac{E_1\nu_{21}}{1-\nu_{23}} & E_2\nu_{23} & E_2 & 0 & 0 & 0 \\ 0 & 0 & 0 & \frac{E_2}{(1+\nu_{23})} & 0 & 0 \\ 0 & 0 & 0 & 0 & 2G_{12} & 0 \\ 0 & 0 & 0 & 0 & 0 & 2G_{12} \end{bmatrix} \tag{12}$$

Expanding the elastic strain energy density $W_{strain} = \frac{\{\varepsilon\}^T[K]\{\varepsilon\}}{2}$ by use of Eq (12), one can obtain

$$W_{strain} = \frac{1}{2}(G_{12}(S)\gamma_{12}^2 + E_2(S)\varepsilon_{22}^2 + G_{12}(S)\gamma_{31}^2 + E_2(S)\varepsilon_{33}^2 + \frac{2E_1\varepsilon_{22}\varepsilon_{11}\nu_{23}}{1-\nu_{23}} + \frac{2E_1\varepsilon_{33}\varepsilon_{11}\nu_{23}}{1-\nu_{23}} + \frac{E_1\varepsilon_{11}^2}{1-\nu_{23}} + 2E_2(S)\varepsilon_{22}\varepsilon_{33}\nu_{23} - \frac{E_1\varepsilon_{11}^2\nu_{23}}{1-\nu_{23}} + \frac{E_2(S)\gamma_{23}^2}{2(1+\nu_{23})}) \tag{13}$$

Where $\gamma_{ij} = 2\varepsilon_{ij}$ are the engineering (as opposed to tensorial) definitions of shear strain. Note that, only the transverse Young's modulus, E_2, and shear modulus, G_{12}, are functions

of S, per the previously stated assumptions about the matrix damage modes. The damage moduli are related to the virgin (undamaged) moduli E_{20} and G_{120} and the internal state variable S through a pair of matrix microdamage functions e_s and g_s that are obtained from three coupon experiments.

$$E_2 = E_{20} e_s(S) \tag{14}$$

$$G_{12} = G_{120} g_s(S) \tag{15}$$

The components of the stiffness matrix $K_{22} = K_{33}$ and $K_{55} = K_{66}$ for all S so the stiffness matrix remains transversely isotropic even as damage evolves. This type of damage evolution mimics a spherical type of damage growth, although E_{11} is assumed unaffected due because of the presence of the fiber, rather than planar cracks. This assumption was used to simplify the formulation and implementation of this damage model by eliminating the requirement of defining a crack orientation in 3D space.

Substituting Eq. (13) and Eq. (1) into Eq (2) results in an evolution equation that can be used to solve for S for a given strain state. Following [15] a reduced internal state variable S_r can be used in place of S, so that the experimental data can be easily fit with a polynomial

$$S_r = S^{\frac{1}{n}} \tag{16}$$

With Eq (16) and the chain rule for derivatives, Eq (2) can be written as follows

$$\frac{\partial W_{strain}}{\partial S_r} = -nS_r^{n-1} \tag{17}$$

In the literature [15] [6] [8], both E_2 and G_{12} are expressed by 5th order polynomial of S_r. In this research, two combinations of polynomials for E_2 and G_{12} are used. In the first method, E_2 is a 6th order polynomial and G_{12} is a 5th order polynomial. In the second method, E_2 is a 5th order polynomial and G_{12} is a 5th order polynomial. In the third method, E_2 is a 5th order polynomial and G_{12} is a 5th order polynomial but a different exponent (n= $\frac{1}{4}$) in Eq 17 is used. The summary of the functional for E_2 and G_{12} is listed in Table 1. In this section, derivation with regards to 6th order polynomial for E_2 and 5th order polynomial for G_{12} will be presented. The results for 5th order polynomial for E_2 and 5th order polynomial for G_{12} can be easily be deduced from the results of the first method. E_2 as a 6th order polynomial function in S_r and G_{12} as a 5th order polynomial function in S_r are expressed as follows:

	Polynomial order of E_2	Polynomial order of G_{12}	value of n in Eq 17
First method	6	5	3
Second method	5	5	3
Third method	5	5	4

Table 1: Summary of polynomial for E_2 and G_{12} for three methods

$$E_2 = E_{20}(e_0 + e_1S_r + e_2S_r^2 + e_3S_r^3 + e_4S_r^4 + e_5S_r^5 + e_6S_r^6) \tag{18}$$

$$G_{12} = G_{120}(g_0 + g_1S_r + g_2S_r^2 + g_3S_r^3 + g_4S_r^4 + g_5S_r^5) \tag{19}$$

Substituting Eq (18) and Eq (19), Eq (13) into the evolution equation Eq (17), one can obtain the evolution equation in terms of a fifth order polynomial for S_r expressed as the following

$$a_0 + a_1 S_r + a_2 S_r^2 + a_3 S_r^3 + a_4 S_r^4 + a_5 S_r^5 = 0 \tag{20}$$

where

$$a_0 = \frac{g_1 G_{120}(\gamma_{12}^2 + \gamma_{31}^2)}{2} + \frac{e_1 E_{20}(\gamma_{23}^2)}{4} + \frac{e_1 E_{20}(\varepsilon_{22}^2 + \varepsilon_{33}^2)}{2} + e_1 E_{20}\varepsilon_{22}\varepsilon_{33}\nu_{23} \tag{21}$$

$$a_1 = g_2 G_{120}(\gamma_{12}^2 + \gamma_{31}^2) + e_2 E_{20}(\varepsilon_{22}^2 + \varepsilon_{33}^2) + 2e_2 E_{20}\varepsilon_{22}\varepsilon_{33}\nu_{23} + \frac{e_2 E_{20}\gamma_{23}^2}{2(1+\nu_{23})} \tag{22}$$

$$a_2 = 3 + \frac{3}{2} g_3 G_{120}(\gamma_{12}^2 + \gamma_{31}^2) + \frac{3}{2} e_3 E_{20}(\varepsilon_{22}^2 + \varepsilon_{33}^2) + 3e_3 E_{20}\varepsilon_{22}\varepsilon_{33}\nu_{23} + \frac{3}{4}\frac{e_3 E_{20}\gamma_{23}^2}{(1+\nu_{23})} \tag{23}$$

$$a_3 = 2g_4 G_{120}(\gamma_{12}^2 + \gamma_{31}^2) + 2e_4 E_{20}(\varepsilon_{22}^2 + \varepsilon_{33}^2) + 4e_4 E_{20}\varepsilon_{22}\varepsilon_{33}\nu_{23} + \frac{e_4 E_{20}\gamma_{23}^2}{(1+\nu_{23})} \tag{24}$$

$$a_4 = \frac{5}{2} g_5 G_{120}(\gamma_{12}^2 + \gamma_{31}^2) + \frac{5}{2} e_3 E_{20}(\varepsilon_{22}^2 + \varepsilon_{33}^2) + 5e_5 E_{20}\varepsilon_{22}\varepsilon_{33}\nu_{23} + \frac{5}{4}\frac{e_5 E_{20}\gamma_{23}^2}{(1+\nu_{23})} \tag{25}$$

$$a_5 = 3e_6 E_{20}(\gamma_{22}^2 + \gamma_{33}^2) + 6e_6 E_{20}\varepsilon_{22}\varepsilon_{33}\nu_{23} + \frac{3e_6 E_{20}\gamma_{23}^2}{2(1+\nu_{23})} \tag{26}$$

The 5th order polynomial for S_r in Eq (20) is solved by the method in [17]. The solutions contain both complex numbers and real numbers and the complex numbers are excluded from being used as values for the reduced internal state variable, S_r.

Experimental validation

Characterizing internal state variable from Compressive tests

A compressive test is conducted where load is applied in the transverse direction of uni-directional composites to establish the relation between the transverse modulus and the internal state variable. A compressive test is conducted in [45] composites to to establish the relation between the shear modulus and the internal state variable. Compressive tests were performed on a servo-hydraulic universal test machine by Shimadzu Inc. An image of the experimental setup is shown in Figure 3

The width of the specimen is 71.15 mm and the height of the specimen is 71.26 mm. The thickness of the specimens ranges from 7.8 mm. For each experiment, two strain gages were attached to the specimen (back to back) aligned with the loading direction and one in the transverse direction on one side. The purpose of using two strain gages in the loading direction is to monitor any unwanted bending that may occur during the compression loading. In a compressive test, A small pre-load is imposed on the specimen and all strain gages are zeroed at this state. The strain gage readings and the load cell readings are acquired at 4Hz, while the axial cross-head movement rate imposed on the specimen is 0.020 mm/sec.

The stress-strain curve for load applied in the transverse direction of composites is in Fig-

ure 4. With Figure 4, at a specific location, the corresponding internal state variable (or reduced internal state variable), S (or S_r), and degraded transverse modulus can be calculated. The coefficients for polynomial e_s related transverse modulus and reduced internal state variable are summarized in Table 3. A compressive test is conducted on a $[45]_{16}$ composite to extract the shear modulus and shear strain. The stress-strain curve for shear modulus is in Figure 5. The corresponding internal state variable (or reduced internal state variable), S (or S_r), and degraded shear modulus can be calculated. The coefficients for polynomial g_s related shear modulus and reduced internal state variable are summarized in Table 3. The plot of polynomial e_s for transverse modulus and the plot of polynomial g_s for shear modulus are in Figure 6 and Figure 7.

e_0	1	g_0	1
e_1	0.137676	g_1	-0.0837419
e_2	-0.0349585	g_2	0.00756448
e_3	0.00286427	g_3	-0.000310913
e_4	-0.000103419	g_4	5.215e-6
e_5	1.357e-6	g_5	-9.9161e-8

Table 2: The coefficients of e_i and g_i for unidirectional composites

Three point bending tests and simulations

The material parameters extracted from the coupon tests are implemented in 3D Schapery's theory for predicting unidirectional composites under three point bending tests. The composites plate of dimension 147.5 mm by 120 mm by 6.2 mm and the setup of the three point bending test is in Figure 8. The 3D extension of Schaperys theory for unidirectional composites is implemented in a UMAT user defined subroutine in Abaqus[18]. The

stress-strain curves used in simulations for E_2 and G_{12} are in Figure 4 and Figure 5. These stress-strain curves exhibit post-peak strain softening. It has been well documented that numerical simulations utilizing constitutive laws exhibiting post-peak strain softening suffer from pathological mesh dependence [19]. It should be noted that Schaperys theory has previously been enhanced to eliminate pathological mesh dependence through regularization of the energy dissipated in the post-peak regime via introduction of a characteristic element length and additional internal state variables[6]. However, that formulation is omitted herein to focus on extension of only the microdamage model to 3D.

The unloading path at any point on the stress-strain curve is assumed to follow a line connecting the current point and the origin (secant). Thus, the transverse stiffness and shear stiffness, as a function of the internal state variable S, can be calculated.

$S_r = S^{\frac{1}{3}}$ is used following [15] [6], as a reduced internal state variable for $e_S(S_r)$ and $g_S(S_r)$ in Figure 6 and Figure 7. In each step during the simulations, an incremental strain is given, and with the information given above, the corresponding S_r at this step can be calculated from Eq (20). The transverse modulus and shear modulus can then be calculated with Eq (18) and Eq (19) with the coefficients in Table 3 and used to update the integration point stresses, satisfying equilibrium. The comparison of simulations with four tests are in Figure 9. The simulations and experimental results show good agrement before the failure occurs.

Objectivity

First method: sixth order polynomial for $\mathbf{e}_S(S_r)$,fifth order polynomial for $\mathbf{g}_S(S_r)$, $S_r = S^{\frac{1}{3}}$

This 3D extension of Schaperys theory for unidirectional composites is implemented in a UMAT user defined subroutine in Abaqus[18]. The stress-strain curves used in simulations for E_2 and G_{12} are in Figure 10 and Figure 11. These stress-strain curves exhibit post-peak strain softening. It has been well documented that numerical simulations utilizing constitutive laws exhibiting post-peak strain softening suffer from pathological mesh dependence [19]. It should be noted that Schaperys theory has previously been enhanced to eliminate pathological mesh dependence through regularization of the energy dissipated in the post-peak regime via introduction of a characteristic element length and additional internal state variables[6]. However, that formulation is omitted herein to focus on extension of only the microdamage model to 3D.

The unloading path at any point on the stress-strain curve is assumed to follow a line connecting the current point and the origin (secant). Thus, the transverse stiffness and shear stiffness, as a function of the internal state variable S, can be calculated. In this first method, $S_r = S^{\frac{1}{3}}$ is used (see Table 1), following [15] [6], as a reduced internal state variable for $\mathrm{e}_S(S_r)$ and $\mathrm{g}_S(S_r)$ in Figure 12 and Figure 13. A sixth order polynomial, $\sum_{i=0}^{6} e_i Sr^i$ is used to interpolate both e_S and a 5th order polynomial $\sum_{i=0}^{5} g_j Sr^j$ is used to interpolate g_S. The coefficients of e_i and g_i are summarize in Table 3. In each step during the simulations, an incremental strain is given, and with the information given above, the corresponding S_r at this step can be calculated from Eq (20). The transverse modulus and shear modulus can

then be calculated with Eq. (18) and Eq. (19) with the coefficients in Table 1 and used to update the integration point stresses, satisfying equilibrium.

e_0	1	g_0	1
e_1	0.0793859	g_1	0.0698501
e_2	-0.447837	g_2	-0.406715
e_3	0.200224	g_3	0.144906
e_4	-0.0716981	g_4	-0.0465796
e_5	0.011131	g_5	0.00564894
e_6	1.02441^{-6}		

Table 3: The coefficients of e_i and g_i for the first method

Second Method: fifth order polynomial for $\mathbf{e}_S(S_r)$,fifth order polynomial for $\mathbf{g}_S(S_r)$, $S_r = S^{\frac{1}{3}}$

In the second method, a 5th order polynomial, $\sum_{i=0}^{5} e_i Sr_i$ and a 5th order of polynomial $\sum_{j=0}^{5} g_j Sr_j$ is used for both e_S and g_S, similar to [15] [6]. The coefficients are summarized in Table (4). The E_2 and G_{12} as a function of reduced internal state variable for $e_S(S_r)$ and $g_S(S_r)$ are in Figure 14 and Figure 15

It is to be noted that when E_2 and G_{12} are both expressed as 5th order polynomial, Eq (20) has to be modified to the following

$$a_0 + a_1 S_r + a_2 S_r^2 + a_3 S_r^3 + a_4 S_r^4 = 0 \tag{27}$$

That is, only a_0 to a_4 are Eq (27) is required to obtain the state value at each step. The expressions for a_0 to a_4 are the same as those from Eq (21) to Eq (25)

e_0	1	g_0	1
e_1	0.0698501	g_1	0.0698501
e_2	-0.406715	g_2	-0.406715
e_3	0.144906	g_3	0.144906
e_4	-0.0420695	g_4	-0.0420695
e_5	0.00564894	g_5	0.00564894

Table 4: The coefficients of e_i and g_i for the second method

Third method: fifth order polynomial for $\mathbf{e}_S(S_r)$,fifth order polynomial for $\mathbf{g}_S(S_r)$, $S_r = S^{\frac{1}{4}}$

In the third method, instead of using $S_r = S^{\frac{1}{3}}$ as in the literature [15] [6], $S_r = S^{\frac{1}{4}}$ is introduced as the reduced internal state variable that is the argument for the transverse and shear microdamage functions used to represent the input data and formulate the equations for progressive failure. To accommodate this change, Eq (23) has to be modified to Eq (28), and Eq (24) has to be modified to Eq (29), whereas Eq (21) , Eq (22), Eq (25), and Eq (26) remain the same.

$$a_2 = \frac{3}{2}g_3 G_{120}(\gamma_{12}^2 + \gamma_{31}^2) + \frac{3}{2}e_3 E_{20}(\varepsilon_{22}^2 + \varepsilon_{33}^2) + 3e_3 E_{20}\varepsilon_{22}\varepsilon_{33}\nu_{23} + \frac{3}{2}\frac{e_3 E_{20}(\gamma_{23}^2)}{2(1+\nu_{23})} \quad (28)$$

$$a_3 = 4 + 2g_4 G_{120}(\gamma_{12}^2 + \gamma_{31}^2) + 2e_4 E_{20}(\varepsilon_{22}^2 + \varepsilon_{33}^2) + 4e_4 E_{20}\varepsilon_{22}\varepsilon_{33}\nu_{23} + 2\frac{e_4 E_{20}(\gamma_{23}^2)}{2(1+\nu_{23})} \quad (29)$$

A 5th order polynomial, $\sum_{i=0}^{5} e_i Sr_i$ and 5th order of polynomial $\sum_{j=0}^{5} g_j Sr_j$, are used to interpolate e_S and g_S. The coefficients for $\mathrm{e}_S(S_r)$ and $\mathrm{g}_S(S_r)$ are listed in Table (5)

The transverse stiffness microdamage function e_S, as a function of S_r, is shown in Figure 16 and shear modulus microdamage function g_S as a function of S_r in Fig 17. Eq (27) is

e_0	1	g_0	1
e_1	0.0750464	g_1	0.0750464
e_2	-0.203932	g_2	-0.203932
e_3	-0.136793	g_3	-0.136793
e_4	0.0404142	g_4	0.0404142
e_5	-0.00313515	g_5	-0.00313515

Table 5: The coefficients of e_i and g_i for the third method

used to obtain the state value where the expression of a_0 to a_4 is the same as that in Eq (21) to Eq (25)

Simulation Results and Discussion

To compare influence of these three different forms for the matrix microdamage functions on the non-linear response of a composite, finite element simulations of a 10 in. x 10 in. x 0.4 in. unidirectional composite panel with a central circular notch of radius of 0.5 in. under compression, shown in Fig 18, are conducted. Compressive displacement is imposed along the x direction, aligned with the fiber direction. It is noted that the range of state variable within composites from the first method and the second method is between 0 and 2.2 and the range of the state variable within composites from the third method is between 0 and 1.8 (to be consistent with the definition from Figs 12 -Fig 17). If the calculated S_r from Eq. (20) is not within the allowed range, the value will not be used in the computation in the UMAT subroutine. The comparison of stress versus strain curve for three methods is shown in Fig 19. It can be seen that the initial slope of curve is close to the stiffness of fiber as the compression is conducted along the longitudinal direction. Degradation of the transverse and shear moduli is activated by the transverse and shear strain induced in the

finite element. The maximum stress obtained in the first method is close to the maximum stress in the second method and the third method. The maximum load in all three cases is the point at which the FEM solutions diverge due to a large extent of damage and non-linearity in the transverse and shear moduli of the composite. The resulting stress-strain curves for the three methods agree very well, independent of the definition of S_r ($n = \frac{1}{3}$ or $n = \frac{1}{4}$). This indicates objectivity of the evolution equation Eq (17) with respect to the functional form of the microdamage functions.

Objectivity

In continuum mechanics, objectivity is defined as physics parameter that don't change with respect to change of reference coordinate. Here, Objectivity is defined as a physics parameter that don't change when different order of polynomials are used.

The 5th order of polynomial used in the Table 4 where n=3 ($S_{r1} = S^{1/3}$) is the reference case for the discussion of objectivity. The $e(S_{r1})$ in Eq (30) and $g(S_{r1})$ in Eq (31) as a function of S_{r1} are shown in Figure 14 and Figure 15. The coefficients $er1_i$, i=1,5 and $gr1_i$, i=1,5 are directly obtained from the interpolation.

$$e(S_{r1}) = (er1_0 + er1_1 S_{r1} + er1_2 S_{r1}^2 + er1_3 S_{r1}^3 + er1_4 S_{r1}^4 + er1_5 S_{r1}^5) \tag{30}$$

$$g(S_{r1}s) = (gr1_0 + gr1_1 S_{r1} + gr1_2 S_{r1}^2 + gr1_3 S_{r1}^3 + gr1_4 S_{r1}^4 + gr1_5 S_{r1}^5) \tag{31}$$

One can replace the reduced internal state variable $S_{r1} = S^{\frac{1}{3}}$ with a different definition of

the reduced internal state variable $S_{r2} = S^{\frac{1}{4}}$ by replacing S_{r1} with $S_{r2}^{\frac{4}{3}}$. As such, Eq (30) and Eq (31) are rewritten as

$$e(S_{r2}) = (er1_0 + er1_1 S_{r2}^{\frac{4}{3}} + er1_2 S_{r2}^{\frac{8}{3}} + er1_3 S_{r2}^{\frac{12}{3}} + er1_4 S_{r2}^{\frac{16}{3}} + er1_5 S_{r2}^{\frac{20}{3}}) \tag{32}$$

$$g(S_{r2}) = (gr1_0 + gr1_1 S_{r2}^{\frac{4}{3}} + gr1_2 S_{r2}^{\frac{8}{3}} + gr1_3 S_{r2}^{\frac{12}{3}} + gr1_4 S_{r2}^{\frac{16}{3}} + gr1_5 S_{r2}^{\frac{20}{3}}) \tag{33}$$

The order exponents Eq (32) and Eq (33) as functions of S_{r2} are not integers. The solution of the evolution equation becomes more challenging if Eq (32) and Eq (33) are used because the exponents in the equation are not integers.

On the other hand, one can directly obtain the 5th order polynomial by using the curve $e(S_{r2})$ and $g(S_{r2})$ directly from $e(S)$ and $g(S)$ where S is initial internal state variable. The coefficient of 5th order of polynomial after interpolation are in the Table (5) where n=4 and ($S_{r2} = S^{1/4}$)

$$e(S_{r2}) = (er2_0 + er2_1 S_{r2} + er2_2 S_{r2}^2 + er2_3 S_{r2}^3 + er2_4 S_{r2}^4 + er2_5 S_{r2}^5) \tag{34}$$

$$g(S_{r2}) = (gr2_0 + gr2_1 S_{r2} + gr2_2 S_{r2}^2 + gr2_3 S_{r2}^3 + gr2_4 S_{r2}^4 + gr2_5 S_{r2}^5) \tag{35}$$

The comparison of $e(S_{r2})$ in Eq (32) and $e(S_{r2})$ in Eq (34) is shown in Figure 20. The two curves show excellent agreement The evolution equation involves the derivativse of

$e(S_{r2})$ and $g(S_{r2})$. Here, the comparison of derivative of $e(S_{r2})$ in Eq (32) and $e(S_{r2})$ are in Eq (34) is shown in Figure 21. It can be seen that the two curves match very well.

The agreement of $e(S_{r2})$ in Eq (32) and $e(S_{r2})$ in Eq (34) from Figure 20 and the derivative $e(S_{r2})$ in Eq (32) and $e(S_{r2})$ in Eq (34) in Figure 21 are the required conditions to satisfy objectivity of the evolution equation with respect to the functional form of the microdamage functions. Strictly speaking, $e(S_{r2})$ in Eq (32) and $e(S_{r2})$ in Eq (34) are not mathematically equivalent. However,these two functions can be regarded to be equivalent if the differences between the two functions and the corresponding derivative are negligible.

Summary

In this paper, the Schapery's thermodynamically-based work potential theory for laminated composites assuming a state of plane stress is extended to accommodate fully 3D stress and strain fields. In the first part of the work, 3D Schaper's theory for unidirectional composites is used to model unidirectional composites under three point bending. Compressive tests are conducted to obtain the relation between the internal state variable and the transverse modulus, shear modulus. The simulations and experimental results show good agrement before the failure occurs. In the second part of the work, objectivity is studied. Three methods for representing the matrix microdamage functions used to control the degradation of the transverse and shear stiffnesses in Schapery's theory are presented. In these three representations, the order of the polynomial used to fit the data and the value of the exponent utilized in the reduced definition S_r of the microdamage internal state variable S are varied. The simulations of a square, center-notched panel under compression using the three dif-

ferent microdamage function representations are compared. Simulation results show that the polynomial order doesn't affect the maximum stress given the same S_r. The response of composites is not sensitive to the choice S_r (as different exponent of S) as long as the objectivity is satisfied. However, an additional internal state variable may be introduced to represent different failure mechanisms, other than matrix microdamage.

References

[1] Tsai, S. W. and Wu, E. M. . A general theory of strength for anisotropic materials. journal of composite materials. *Journal of Composite Materials*, 5:58–88, 1971.

[2] M.A. Crisfield, Y. Mi, G.A.O. Davies . Progressive delamination using interface elements. *Journal of Composite Materials*, 32(14):1247–1271, 1998.

[3] M.D. Olsson, R. Varizi, D.L. Anderson. Damage in composites: a plasticity approach. *Journal of Composite Materials*, 44:103C116, 1992.

[4] P. Ladeveze, E. Le Dantec. Damage modelling of the elementary ply for laminated composites. *Compos Sci Technol*, 43:257C267, 1992.

[5] V.K. Williams, R. Varizi, A. Poursartip. A physically based continuum damage mechanics model for thin laminated composite structures. *Int J Solids Struct*, 40:2267C2300, 2003.

[6] Pineda, E. J., A. M. Waas. Numerical implementation of a multiple-isv thermodynamically-based work potential theory for modeling progressive damage and failure in fiber-reinforced laminates. *Int. J. Fract.*, 182:93–122, 2013.

[7] Basu, S., A. M. Waas, D. R. Ambur. Compressive failure of fiber composites under multiaxial loading. *J. Mech. Phys. Solids*, 54(3):611–634, 2006.

[8] Pineda, E. J., A. M. Waas, B. A. Bednarcyk, C. S. Collier, P. W. Yarrington. Progressive damage and failure modeling in notched laminated fiber reinforced composites. *Int. J. Fract.*, 158:125–143, 2009.

[9] Chou, T. W. *Microstructural design of fiber composites*, 1992.

[10] Tong, L., Mouritz, A.P., Bannister, M. *3D Fibre Reinforced Polymer Composites*, 2002.

[11] Ashwill TD, Veers PS, Locke J, Contreras I, Griffin D, and Zuteck MD . Concepts for adaptive wind turbine blades. *ASME 2002 Wind Energy Symposium*, Paper No. WIND2002-28:56–69, 2002.

[12] Golzar M,Poorzeinolabedin M . Prototype fabrication of a composite automobile body based on integrated structure. *The International Journal of Advanced Manufacturing Technology*, 49:1037–1045, 2010.

[13] C. R. Cater, X. Xiao, R. K. Goldberg, L. W. Kohlman. Improved subcell model for the prediction of braided composite response. *NASA/TM-2013-217875*.

[14] B. A. Bednarcyk, B. Stier, J.-W. Simon, S. Reese., E. J. Pineda. Meso- and micro-scale modeling of damage in plain weave composites. *Composite Structures*, 121:258–270, 2015.

[15] Lamborn, M. J., R. A. Schapery. A theory of mchanical behaviour of elastic media with growing damage and other changes in structure. *J. Mech. Phys. Solids*, 38(2):1725–1797, 1990.

[16] Sicking, D. L. Mechanical characterization of nonlinear laminated composites with transverse crack growth. *PhD thesis Texas AM University College Station TX*, 1992.

[17] Skowron , Gould . General complex polynomial root solver and its further optimization for binary microlenses. *arXiv:1203.1034*, 2012.

[18] 2013 Users Manual, version 6.13, Dassault Systmes.

[19] Bazant, Zdenek P.; Luigi Cedolin. *Stability of Structures: Elastic, Inelastic, Fracture, and Damage Theories)*. Oxford, 1991.

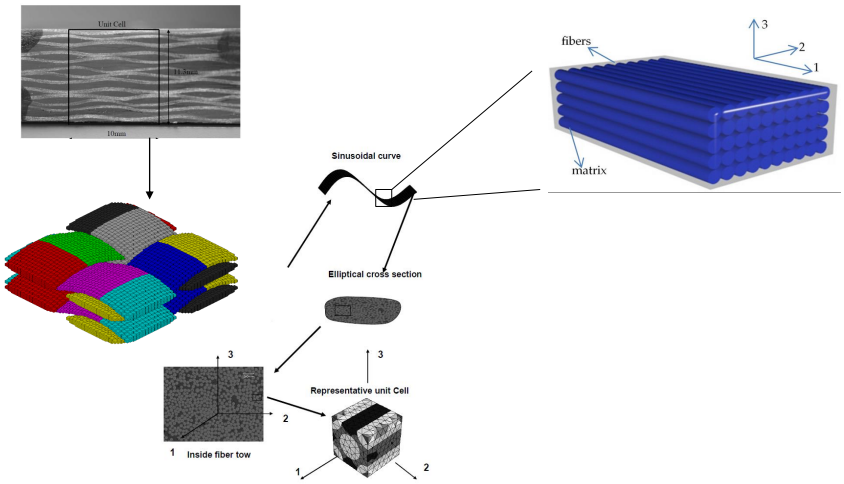

Figure 1: Hierarchical structures of textile composites.

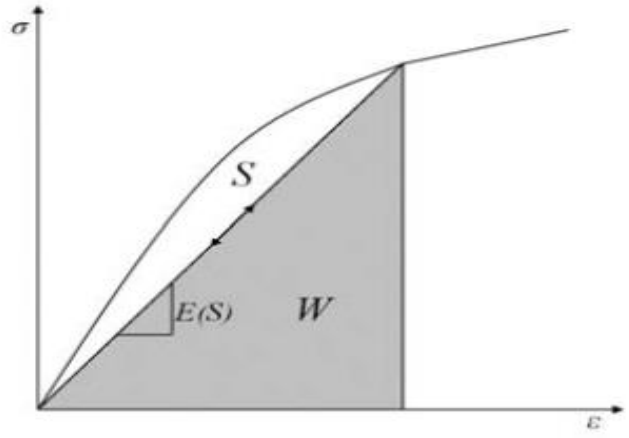

Figure 2: Schematic of state variable S and recoverable energy density W [6]

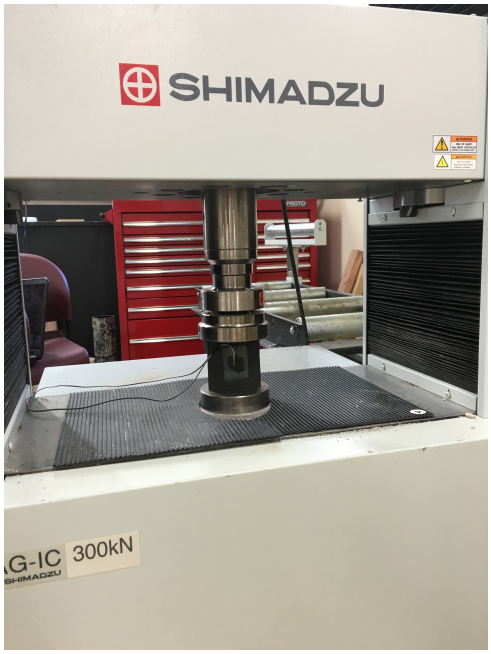

Figure 3: Setup of compression test

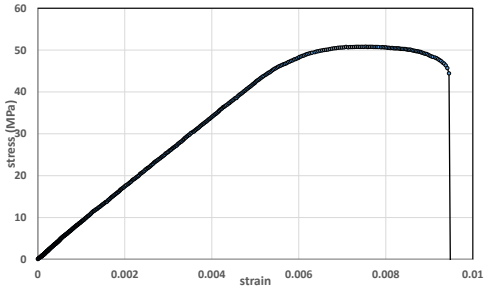

Figure 4: Stress strain curve for transverse modulus

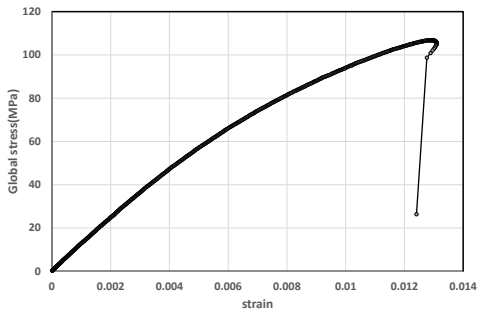

Figure 5: Stress strain curve for shear modulus

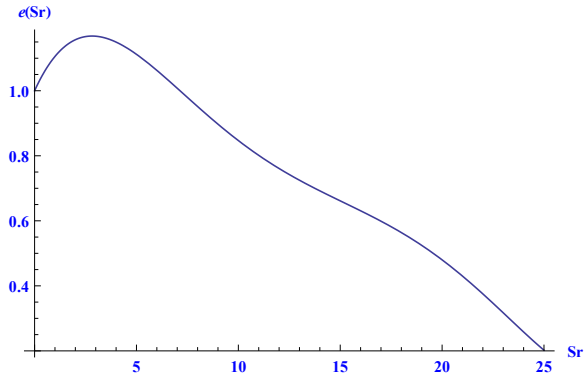

Figure 6: e_s as a function of reduced state variable S_r

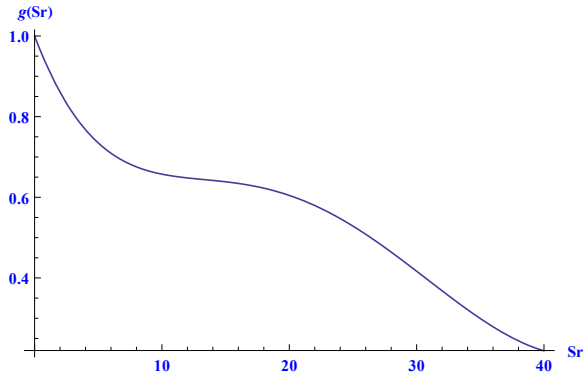

Figure 7: g_s as a function of reduced state variable S_r

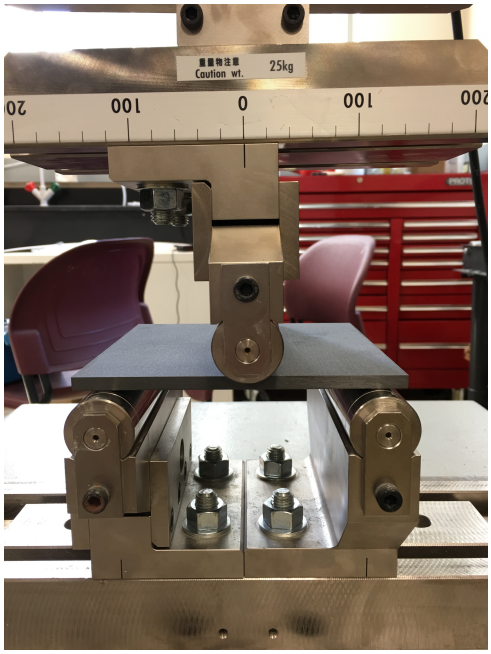

Figure 8: Setup of for three point bending

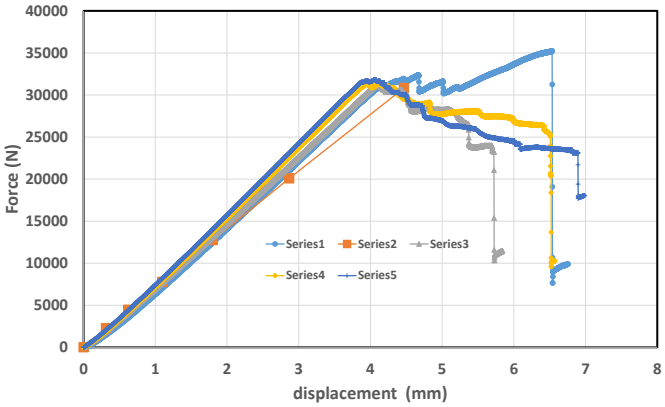

Figure 9: Comparison of simulations with test data of three point bending

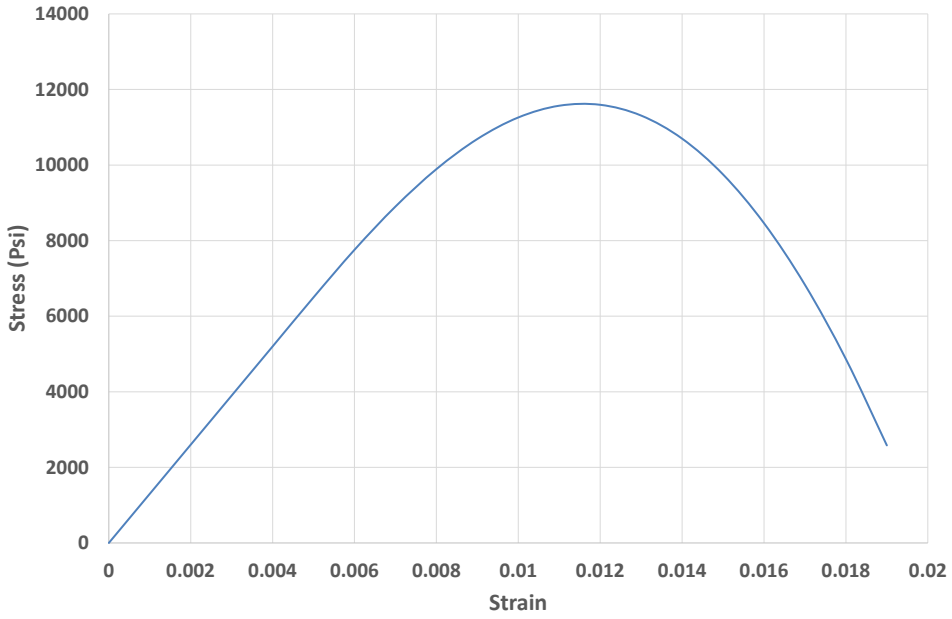

Figure 10: Transverse stress versus transverse strain curve used to obtain functional degradation of transverse Young's modulus E_2

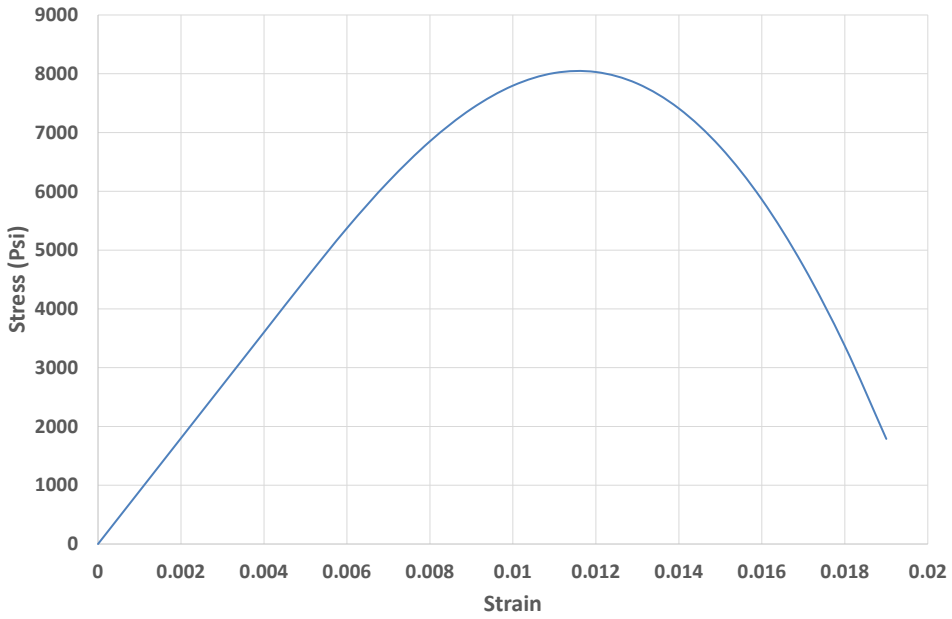

Figure 11: Shear stress versus shear strain used to obtain functional degradation of shear modulus G_{12}

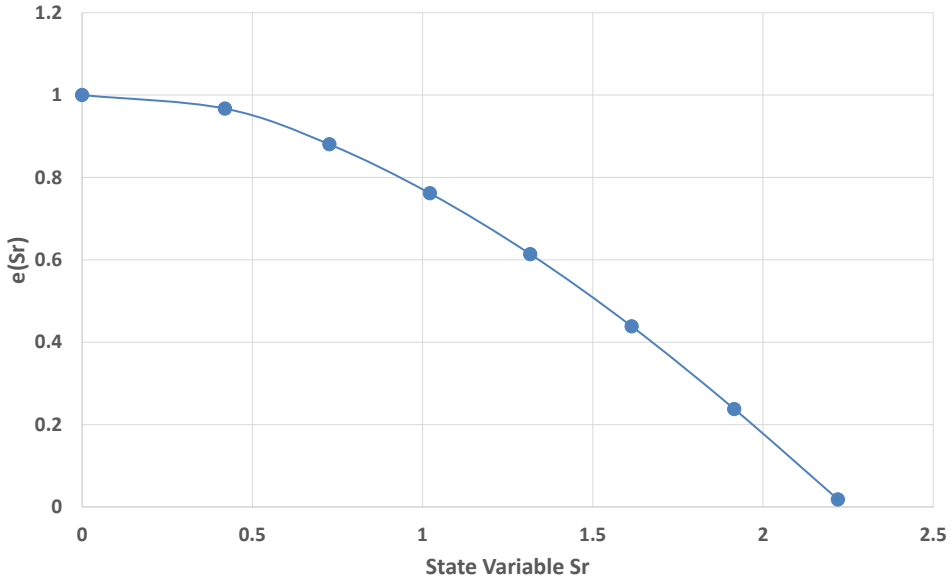

Figure 12: State variable S_r vs e
used to represent degraded transverse Young's modulus E_2 for the first method

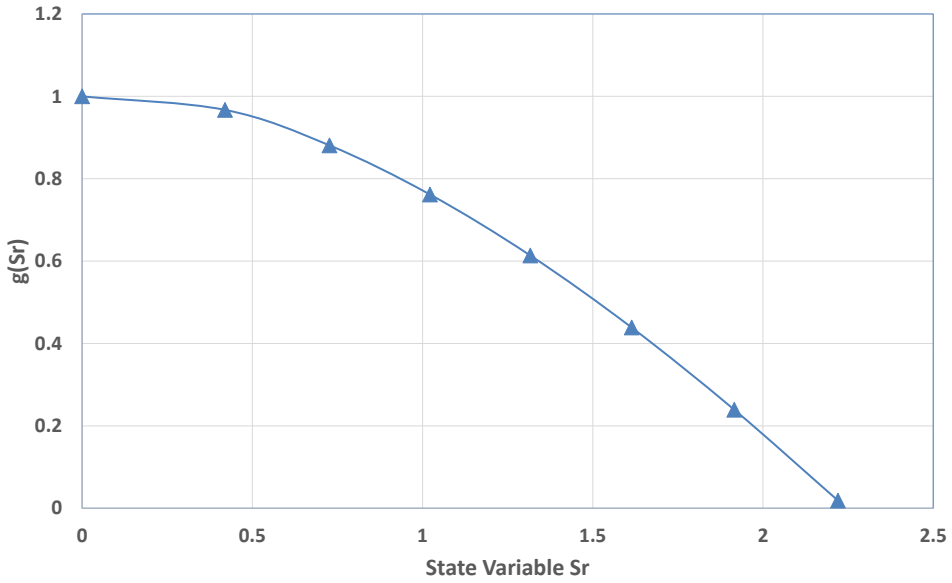

Figure 13: State variable S_r vs g used to represent degraded shear modulus G_{12} for the first method

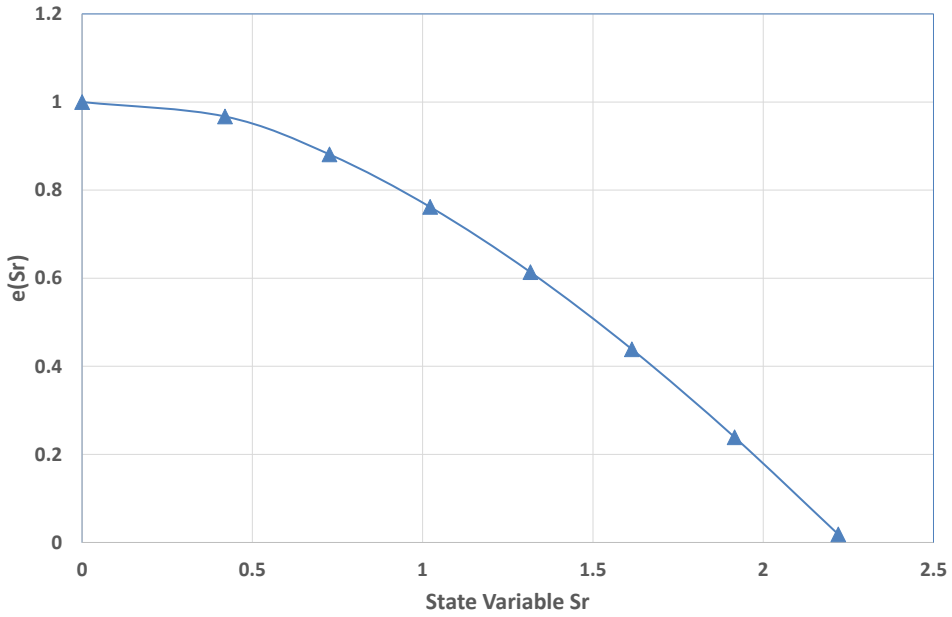

Figure 14: State variable S_r vs e
used to represent degraded transverse Young's modulus E_2 for the second method

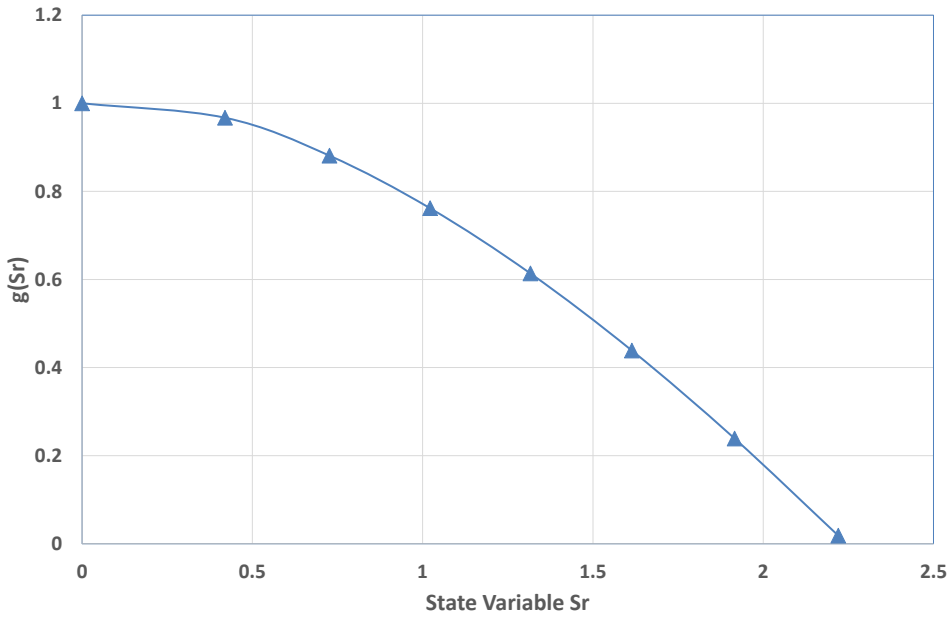

Figure 15: State variable S_r vs g used to represent degraded shear modulus G_{12} for the second method

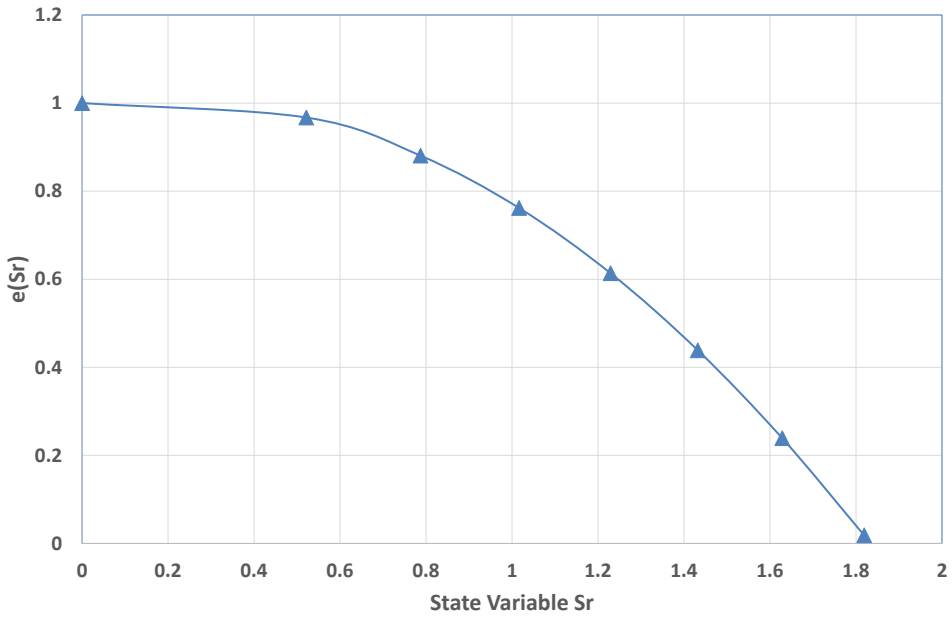

Figure 16: State variable S_r vs e used to represent degraded transverse Young's modulus E_2 for the third method

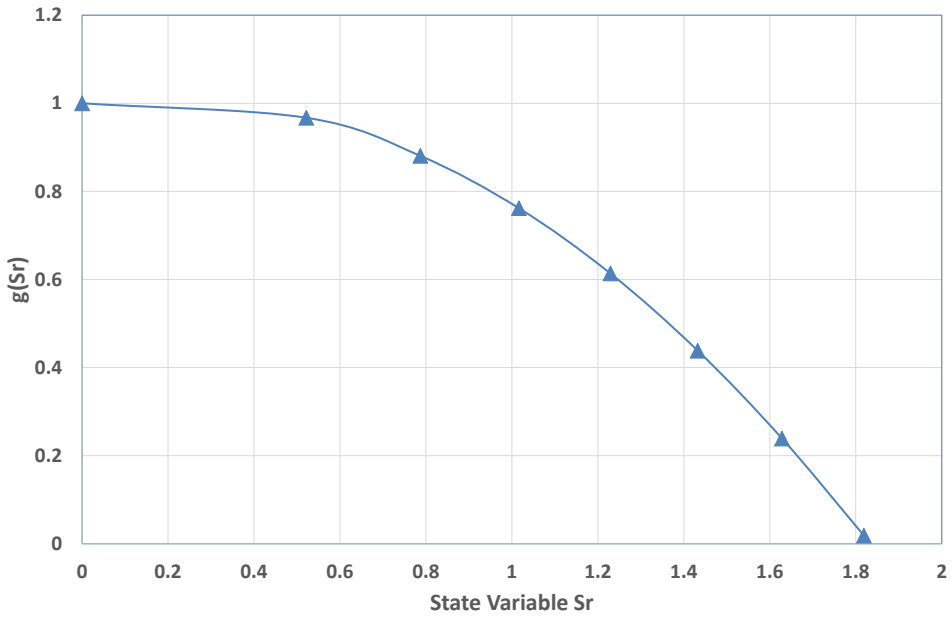

Figure 17: State variable S_r vs g used to represent degraded shear modulus G_{12} for the third method

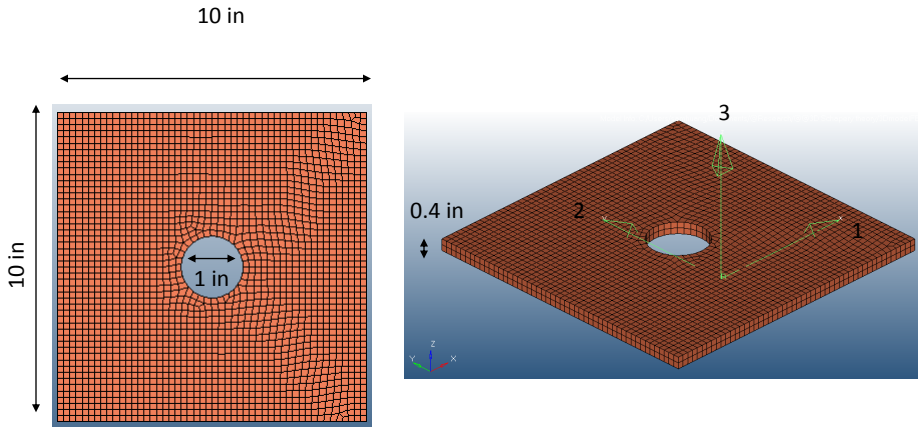

Figure 18: Finite element model of 10 in. by 10 in. by 0.4 in. notched panel

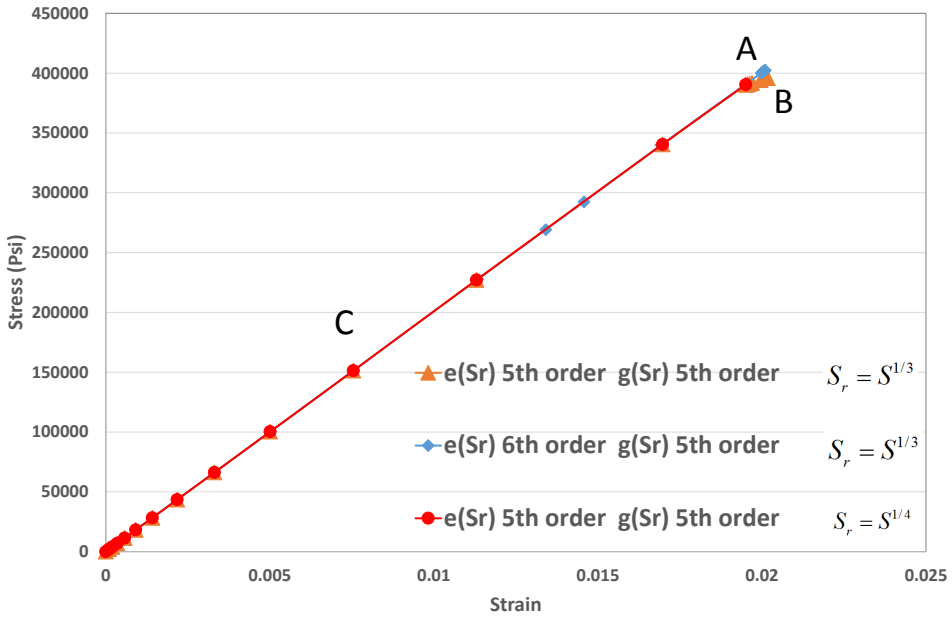

Figure 19: Comparison of simulations of notched square panel under compression for three methods. All three methods produce similar results, indicating objectivity of the microdamage evolution equation with respect the functional form of the microdamage functions.

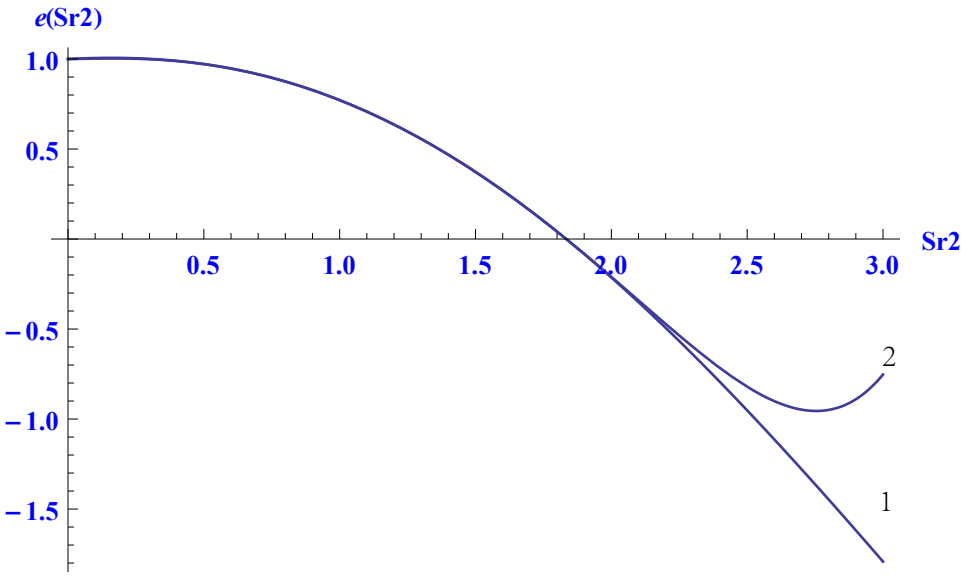

Figure 20: Comparison of internal state variable for two formulation. The curve 1 is from Eq (32) and the curve 2 is from Eq (34)

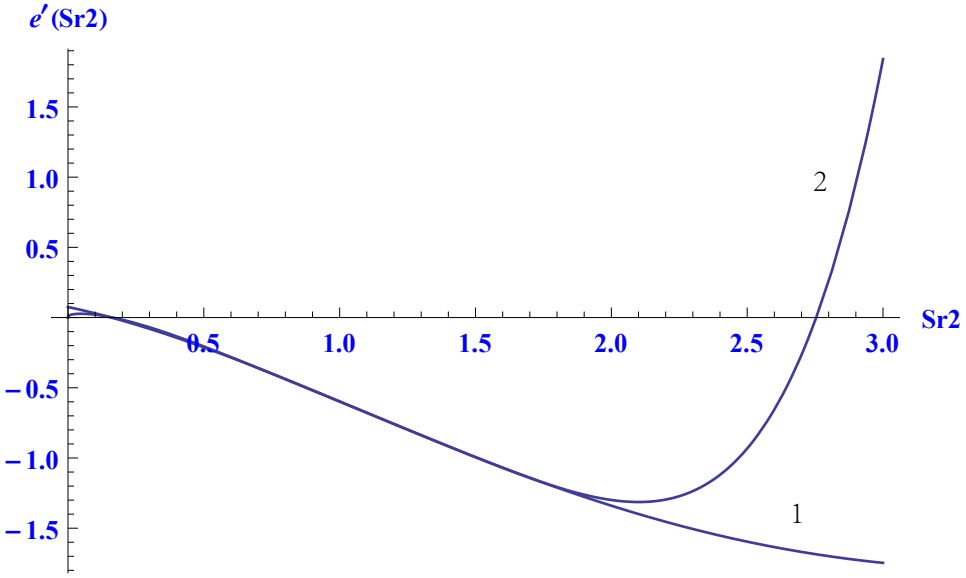

Figure 21: Comparison of derivative of internal state variable for two formulation. The curve 1 is from the derivative of Eq (32) and the curve 2 is from the derivative of Eq (34)